NRIAG JOURNAL OF ASTRONOMY AND GEOPHYSICS
2019, VOL. 8, NO. 1, 144–155
https://doi.org/10.1080/20909977.2019.1626560

Palaeomagnetism of Bahariya iron ores and their genetic implications, North Western Desert, Egypt

A. Awad[a], A. Khashaba[a], E. Abdel Aal[a], H. El-Shayeb[b], A. Khalil[a], I. El-Hemaly[a] and R. Mostafa[a]

[a]National Research Institute of Astronomy and Geophysics, Helwan, Egypt; [b]Menofia University, Egypt

ABSTRACT

Integrated rock magnetic, palaeomagnetic and magnetic fabric studies have been carried out, in order to rely a better understanding of the age and origin of the Bahariya iron ores. A total of 80 oriented block samples were collected from 10 sites covering the three iron mining areas at Bahariya Oasis (El Gedida, Ghorabi and El Harra) within an area located between latitudes (28° 24` to 28° 29`N) and longitudes (29° 02` to 29° 11`E). Rock magnetic measurements reveal that, the main magnetic carrier is the haematite. Goethite and pyrrhotite, that are also present as subordinate constituents in the studied samples. Careful thermal demagnetization successfully enabled the isolation of the characteristic remanent magnetization of primary origin, which yields a magnetic position at Lat. 75.3° N and Long. 137.9° E revealing that, both the ore and host rocks are of the same age. Magnetic fabric studies on these ores indicated that, they are still holding their primary Fabrics of sedimentary origin.

ARTICLE HISTORY
Received 20 February 2019
Revised 15 May 2019
Accepted 30 May 2019

KEYWORDS
Paleomagnetism; magnetic fabric; Bahariya iron ores; north Western Desert; Egypt

1. Introduction

The economic Bahariya iron ore bands and their concretions are located at the lower part of the Lutetian Naqb and Qazzun Formations in the Bahariya Oasis (Said 1990). Origin of the Bahariya iron ores, in previous literatures, ranges from supergene origin, including direct precipitation from the seawater, weathering of the overlying glauconites, and leaching of the underlying Nubia sandstones and basement rocks (e.g. Hussein 1990; El-Aref and Lotfy 1985; Dabous 2002; Baioumy and Hassan 2004; Baioumy et al. 2014) to hypogene origin, including volcanic and hydrothermal sources (e.g. Tosson and Saad 1974; El Sharkawi et al. 1984). Palaeomagnetic characteristics of some Cretaceous Nubian sandstones, and iron ores from Aswan and Bahariya oasis (Schult et al. 1978), show that, the palaeomagnetic pole position of the Bahariya iron ores is significantly different from the Cretaceous pole for the Nubian sandstone and iron ores of the Eastern Desert and in good agreement with the Tertiary poles for Africa.

xIn this work, the authors shed the light on the age and origin of the ore through the interpretation of the palaeomagnetic and magnetic fabric results for the investigated iron ores. The obtained results will help in highlighting many previous literatures that coincide with our result about the source of the ore (e.g. Morsy 1989; Abdel-Monem et al. 2003; Baioumy et al. 2014)

2. Geologic setting

Iron ores in Bahariya Oasis are restricted only to the Cretaceous-Eocene geological units (Figure 1(a)) (Catuneanu et al. 2006 and E. E.; Plyusnina et al. 2016). They are successive types of different modes, formed under subaerial and shallow marine conditions in certain places at certain times; being arranged according to (El-Aref et al. 1999) from base to top as follows:

(a) Bahariya Formation including; Stratiform ironstone bands and lenses confined within the upper member of the Bahariya Formation and cropping out as a result of wrench tectonics.
(b) Naqb and Qazzun Formations including; Strata bound iron developed along the Cretaceous-Eocene unconformity, and Stratiform ironstones of shallow marine environment.
(c) Hamra Formation including; Lateritic glauconitic ore related to alteration of the glaucony facies.

Generall1y, the different types of the economic iron ores of the Lutetian Nagb and Qazzun Formations are obviously observed in the field, based on their constituents, texture and chemical composition. The friable ores (sites F1, F2 and F3) are generally bright yellow and may grade to dark brown or even black, they are soft and friable with earthy lustre. They consist mainly of haematite, goethite and limonite, together with some manganese minerals. The hard ores (sites R1, R2, R3, R4, R5 and R6) are fairly hard,

CONTACT R. Mostafa reem_mostafa2002@yahoo.com National Research Institute of Astronomy and Geophysics, Helwan, Egypt

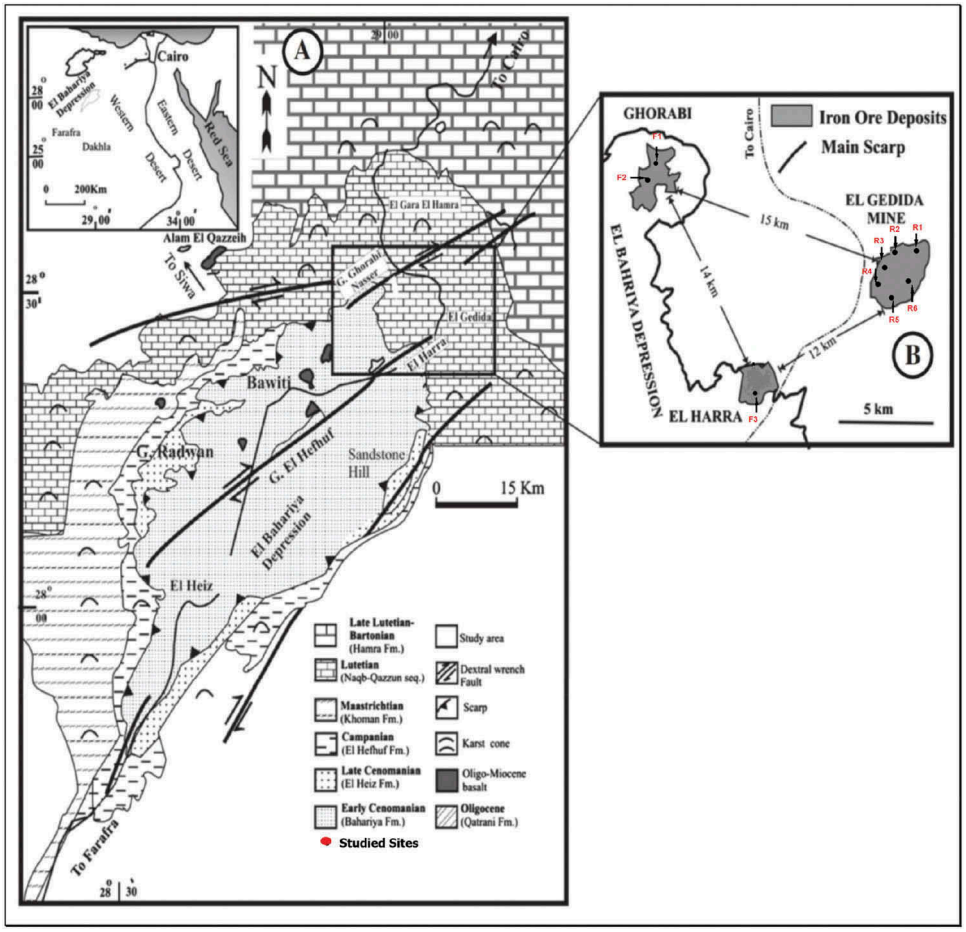

Figure 1. (a) Map of Bahariya oasis (modified after Hermina et al. 1989). (b) Location map of the iron ores mine areas.

crystalline and massive, and has a deep reddish-brown colour and a submetallic lustre. It consists mainly of haematite, with minor amounts of goethite and limonite (Said 1990).

Several possible sources of iron in this region are discussed by many authors, including the following:

El Shazly (1962) suggested an epigenetic-supergene origin in which the deposits have been formed later than the Eocene limestone by supergene solutions.

Tosson and Saad (1974) discussed the actual source of the iron-bearing fluids and found it to be of two types, one related to a volcanogenic source and the other derived from weathering processes.

Helba et al. (2001) recognized four depositional stages of ore development based on ironstone paragenesis suggesting alternating humid and dry conditions.

Baioumy and Hassan (2004) suggested the weathering of overlying glauconites of the Hamra Formation can be source of part of iron in the Bahariya iron ore.

Baioumy et al. (2014) suggested a seawater precipitation of the Bahariya iron ores from the analysing the major, trace, and rare earth elements of different iron ore types from the Ghorabi and El Gedida areas of Bahariya Oasis.

3. Sampling

In order to obtain reliable data; iron ores and their sedimentary host rocks, have been sampled from 10 sites, covering the three major localities of the ore deposits in the Bahariya oasis (El Gedida, Ghorabi and El Harra) areas (Figure 1(b)). Eighty collected hand blocks have been gone, through careful preparation process, to acquire geomagnetically oriented cylindrical specimens, with volume ~10 cm^3 for demagnetization experiments, powder sometimes and small pieces in other times; both for rock magnetic experiments.

Preparation process has taken place in the Palaeomagnetism Laboratory of the National Research Institute of Astronomy and Geophysics, Helwan, Egypt, and in the Palaeomagnetic Lab., Institute of Geophysics, Warsaw, Poland.

4. Rock magnetism

Carefully chosen specimens were subjected to several rock magnetic experiments, including a construction of the Isothermal remanent magnetization (IRM) acquisition curve, Coercivity of remanence, Hysteresis Loops and Curie temperature determination (Thermomagnetic

analysis and Susceptibility versus Temperature), in order to recognize the different magnetic minerals within the studied ores, which are responsible for carrying magnetization.

Figure (2) represents examples of the IRM curves for the studied ores. The constructed curves for the types of the ore specimens show a step gradual to fast increase in the IRM intensity, that possibly due to the high degree of alteration process. Also, non-saturated curves up to the maximum available field (1T) was acquired. This indicates the presence of high coercive magnetic minerals in all the three investigated ore specimens. This hard magnetic mineral could be haematite and/or geothite.

Back Field curves constructed for the same specimens show a gradual decay of the IRM until losing their magnetization nearly at the field from 125 to 525 mT (Figure 3).

The high coercivity of the magnetic carriers confirms the presence of high coercive magnetic mineral as haematite and/or goethite. The obtained results support the results of the IRM experiment.

The hysteresis loops constructed for the specimens of the friable ore, of narrow shape without saturation even in the field of 1000 mT (Figure 4), revealed the presence of hard magnetic mineral(s), where the values of coercivity (Hc) are high ranging from (190 to 260 mT). Such slopes are common, when the specimen has little ferromagnetic material and is rich in iron-bearing phases.

Also, the hysteresis loops constructed for the specimens of the Bahariya iron bands of hard ore are shown in (Figure 4). The higher values of (Hc), which ranging from (180 to 290 mT) confirm the presence of high coercive magnetic mineral (haematite) as the main carrier of magnetization.

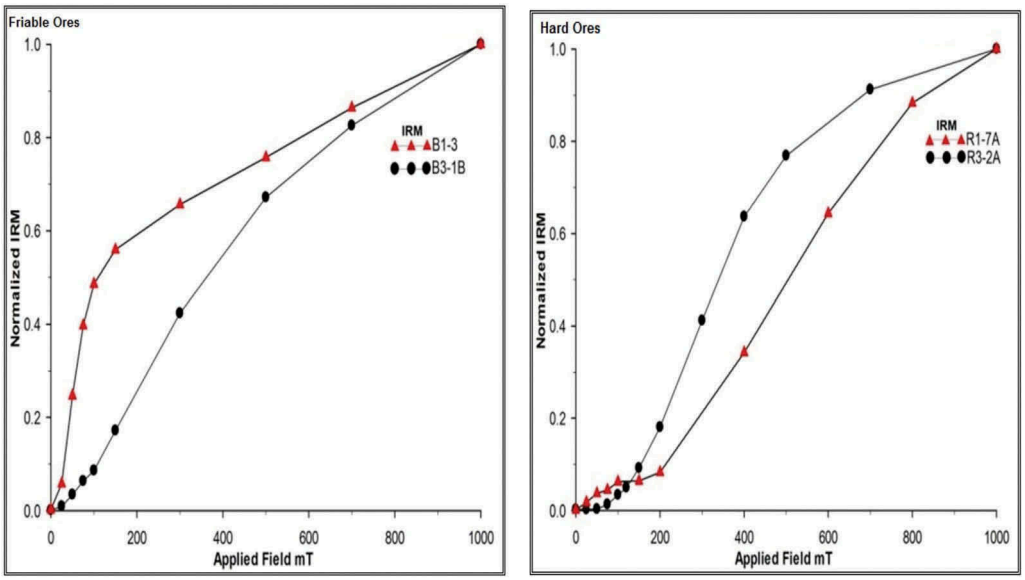

Figure 2. IRM acquisition curves of representative specimens from the Friable and Hard Ores.

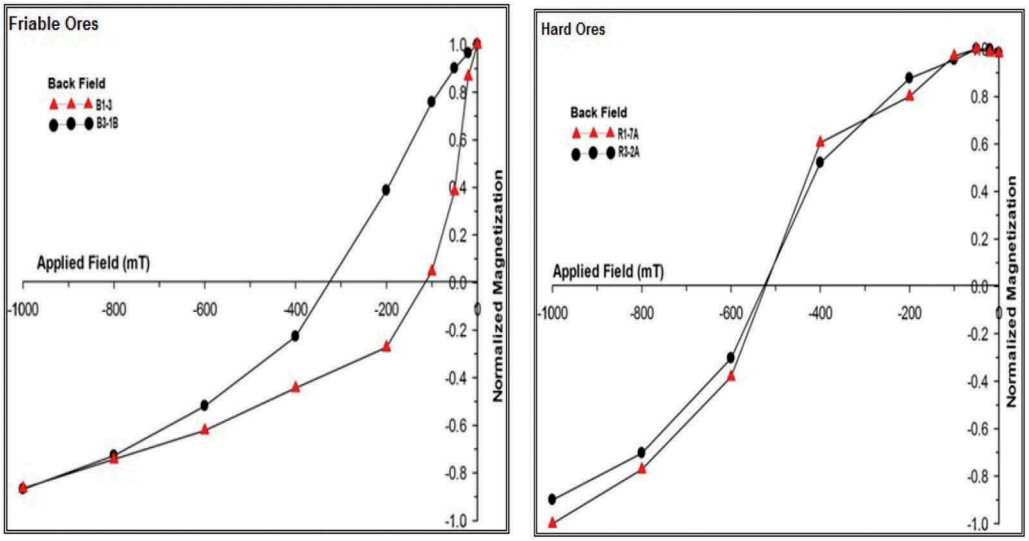

Figure 3. Back-field curves of representative specimens from the Friable and Hard Ores.

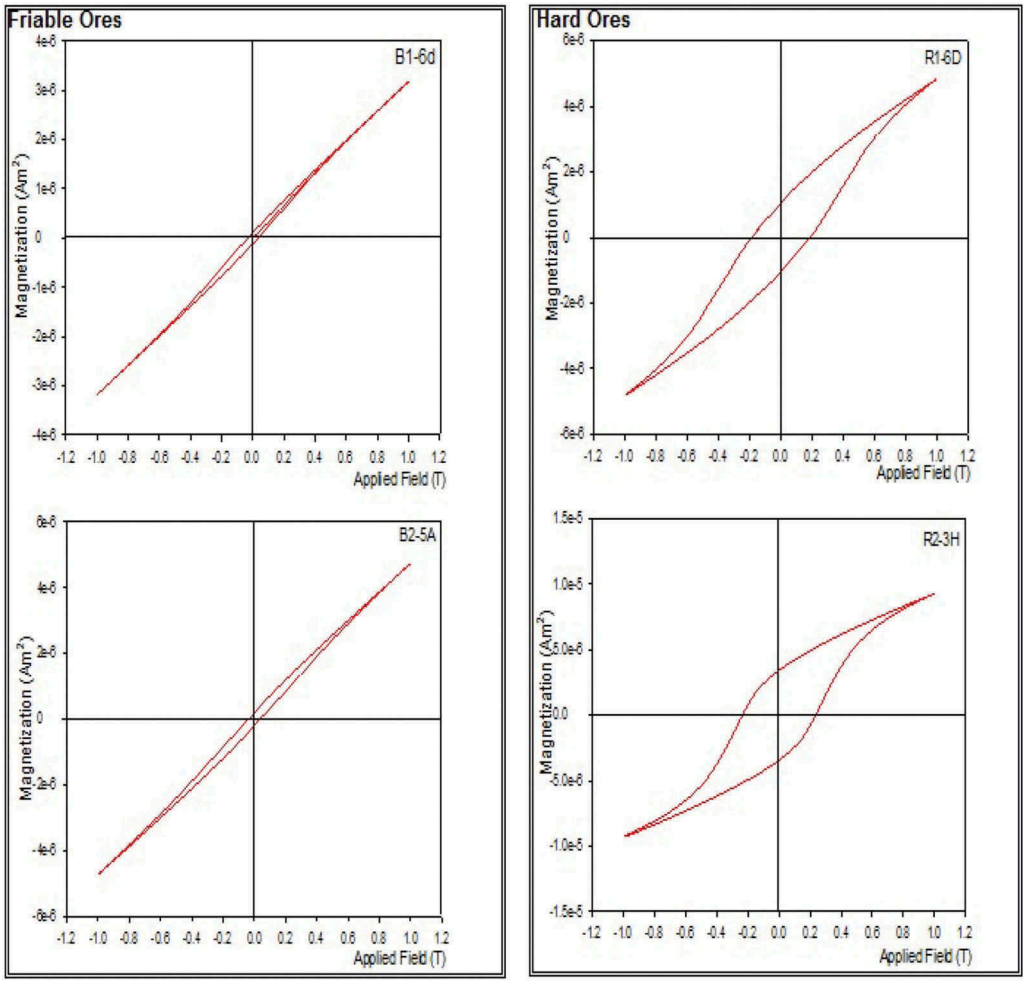

Figure 4. Hysteresis loops for representative specimens from the Friable and Hard Ores.

The loops showed wasp tail shape without saturation even in the field of (1000 mT), reveal the presence of more than one magnetic mineral and the wide incomplete saturation curve reflects haematite presence.

The ratio of saturation remanence to saturation magnetization (Mrs/Ms) is ranging from (0.5 to 0.8), and that of coercivity of remanence to coercive force (Hcr/Hc) is from (1 to 1.5). The ratios of hysteresis parameter are consistent with the dominance of pseudo single domain (PSD) particles in each specimen.

Thermomagnetic analysis reveals blocking temperatures (Tc) of the magnetic minerals present in the rock in its natural state (1st heating curves) and shows changes in the mineral composition implied by heating in the air (2nd heating curves) (Figure 5), the specimen of Friable ore shows abrupt decrease in the magnetization at ~100°C, indicating the presence of geothite, then specimen almost lost its magnetization at 680°C indicating the presence of haematite. Specimens of Hard ores (Figure 5) show gradual decrease till about 680°C. In our work, the identified Curie temperatures value is ~ 680°C (Figure 5).

The susceptibility curves vs temperature of friable ore show stability during the heating process to about 560°C (Figure 6), and then decreased to reach the end of the heating process at 690°C. During cooling cycle, the susceptibility increases sharply and reaches its maximum value at about 560°C, then gradually decreased to reach the end of the process, which supports the previous results that the main magnetic mineral is the haematite.

There is a big difference in susceptibility values between heating and cooling processes which indicates a change in mineral composition due to heating and creation of magnetite.

The curves of hard ore show stability of the K-value during heating and cooling cycles with a peak at about 640°C and 660°C (Figure 6) with sharp increase of the susceptibility curve at the end of the cooling process, these Curie temperatures supports the previous rock magnetic results that the main magnetic mineral is the haematite.

5. Demagnetization

In the present study, the demagnetizations processes have been done using both; Thermal and Alternating Field (AF) techniques. Typical Alternative Field demagnetization process has been done on chosen specimen, representing all the rock units.

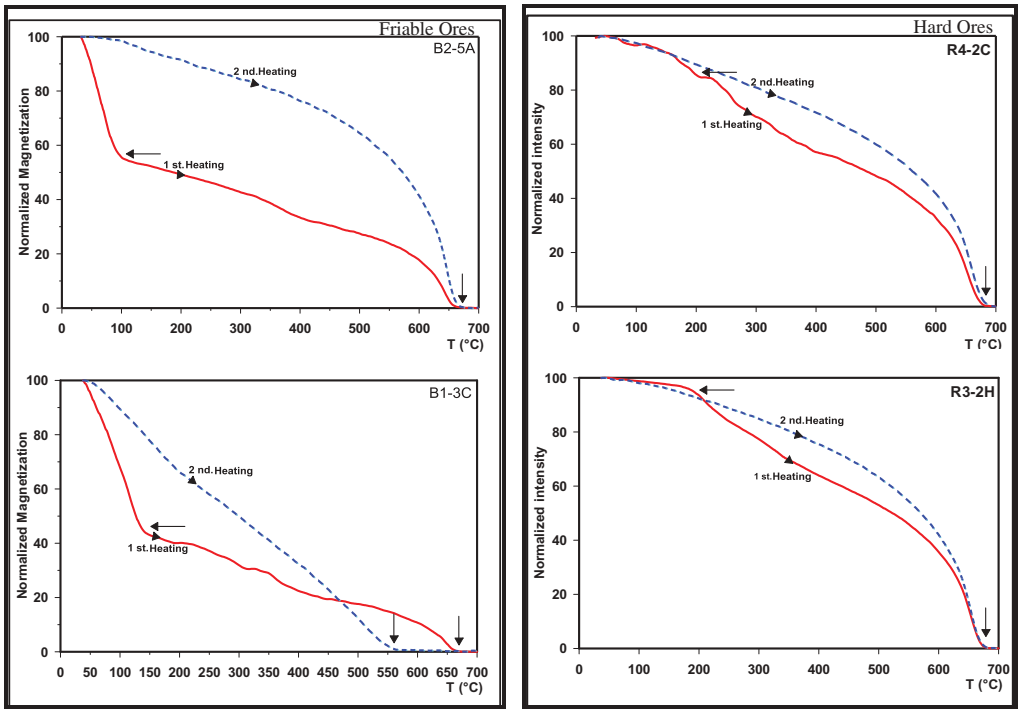

Figure 5. Thermal decay curves for representative specimens from the Friable and Hard Ores.

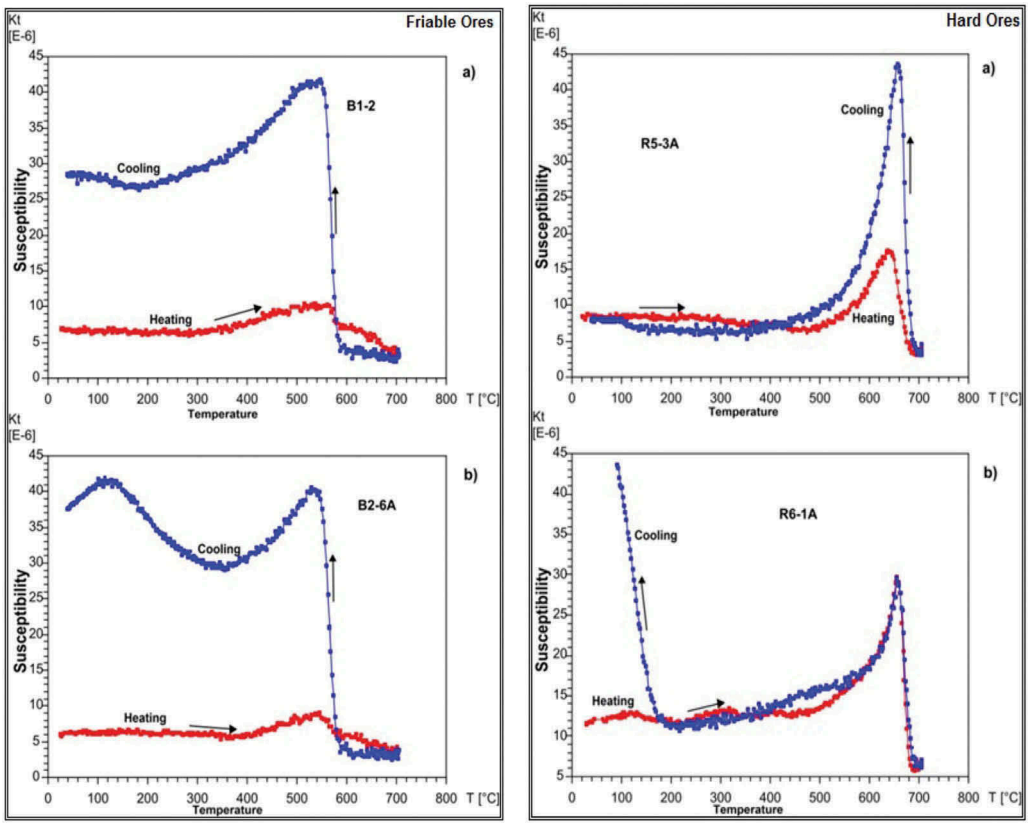

Figure 6. Susceptibility vs Temperature curves for representative specimens from the Friable and Hard Ores.

During the AF treatment, specimens were progressively demagnetized at incremental steps of (5–20) mT up to a peak field of 120 T. The intensity of the NRM is stable during the whole process (Figure 7).

The same process in Thermal Demagnetization was done, most of the collected specimens have been heated in steps of 50°C up to 400°C and then the steps have been reduced to be 25°C up to 700°C. Having haematite as the main magnetic mineral, forced us to focus on the Thermal Demagnetization to be the most effective tool in such case. Stable single magnetization component is clearly identified in most cases, as shown in (Figures 8, 9 &10). After the analysis

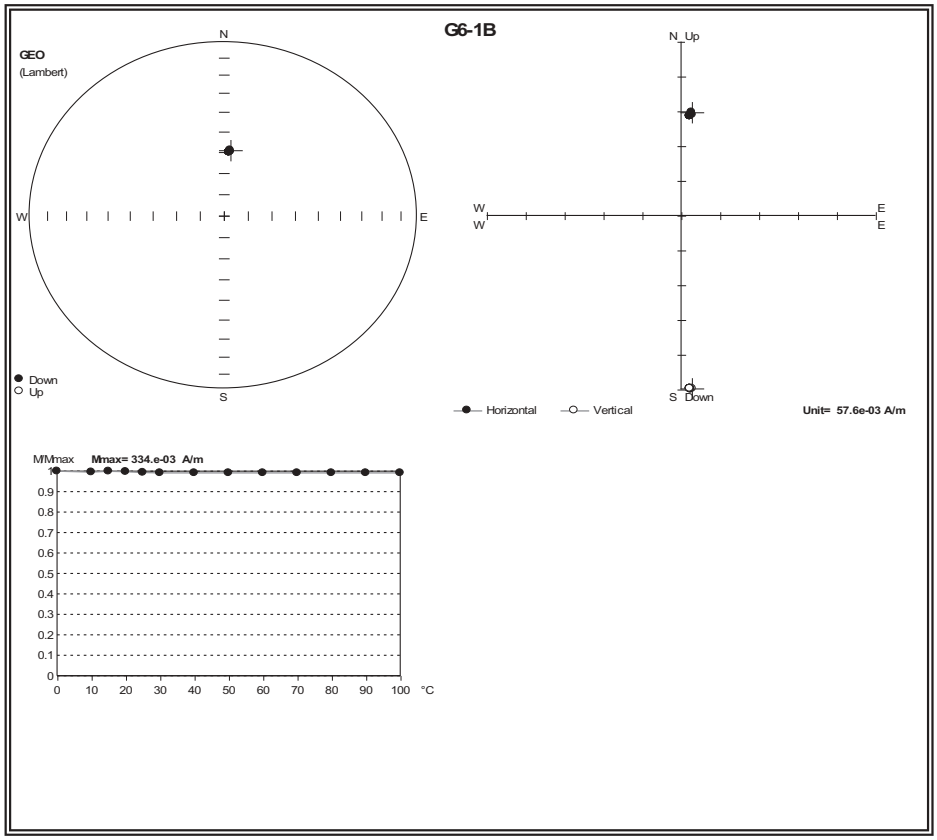

Figure 7. AF demagnetization plots [Stereonet, Zijderveld diagram (Zijderveld 1967) and intensity decay curve] for a representative specimen from the Friable Ores.

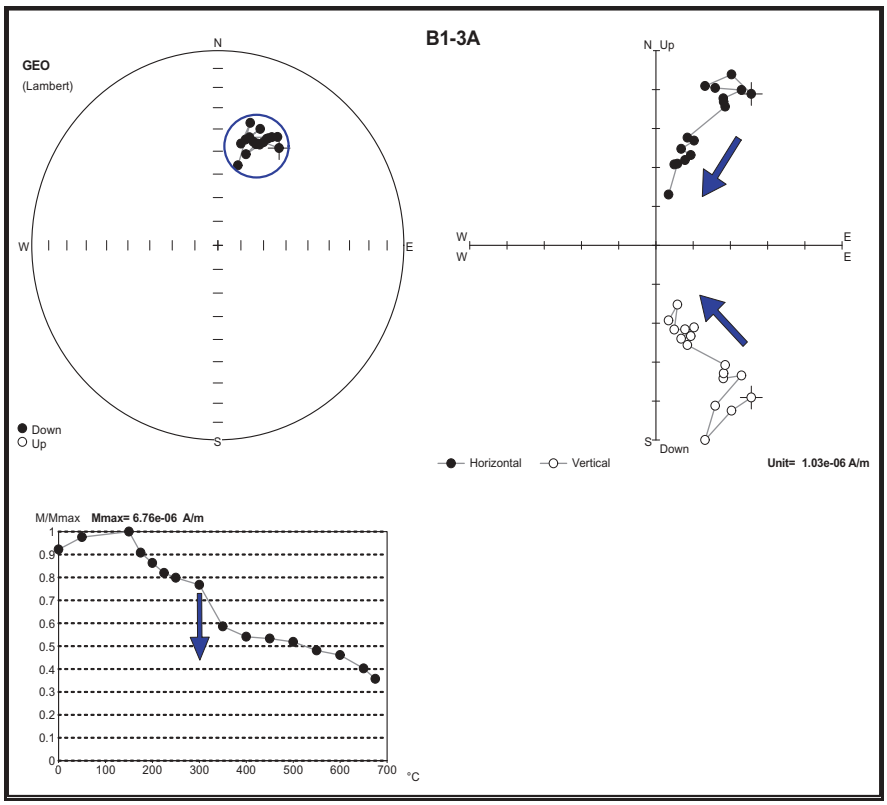

Figure 8. Thermal demagnetization plots [Stereonet, Zijderveld diagram (Zijderveld 1967) and intensity decay curve] for a representative specimen from the Friable Ores.

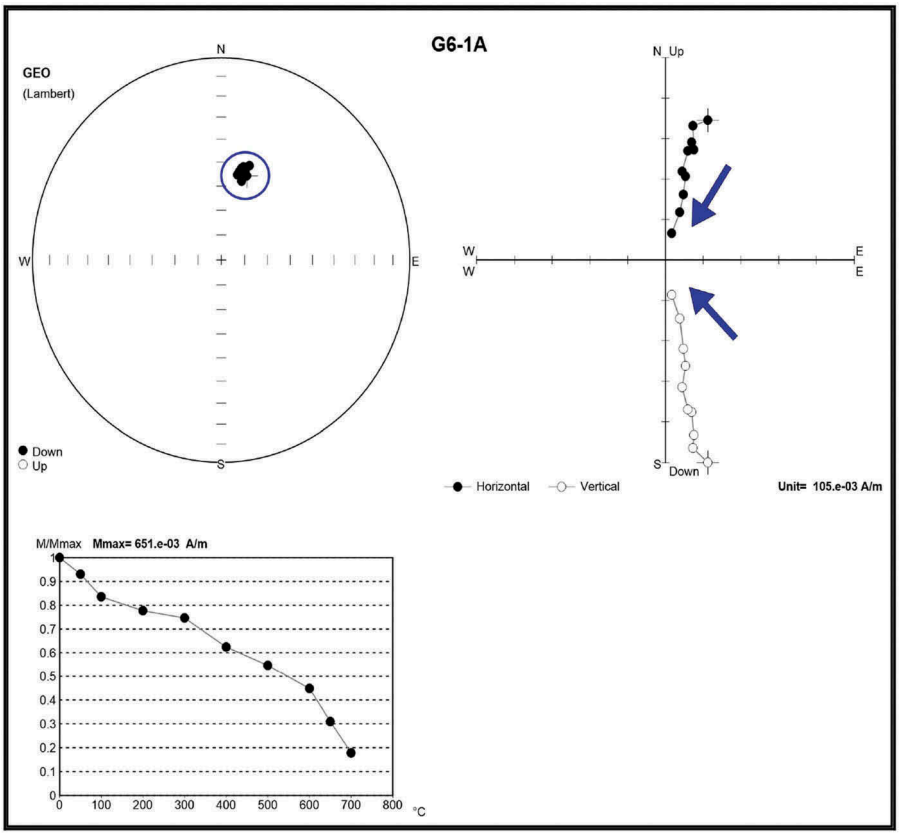

Figure 9. Thermal demagnetization plots for a representative specimen from the Hard Ores (normal polarity).

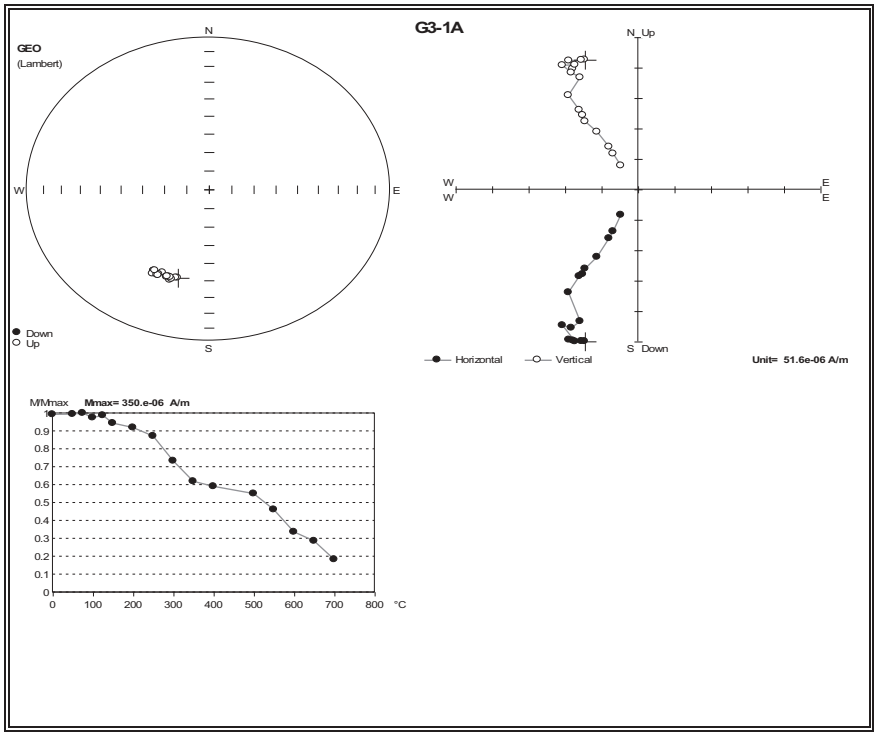

Figure 10. Thermal demagnetization plots for a representative specimen from the Hard Ores (reverse polarity).

of Thermal Demagnetization data of the friable ore; by using Remasoft 3.0 computer program (2018), we found that, there was a single component of NRM of normal polarity. Results of demagnetization are summarized in (Table 1).

The analysis of Thermal Demagnetization data of the hard ore show that, there are two main components of NRM one is of normal polarity, and the other is of reverse polarity. Results of demagnetization are summarized in Table 2.

Table 1. Demagnetization results of the Friable Ores.

Site No.	N	D (°)	I (°)	α_{95} (°)	K	P_Lat. (°N)	P_Long. (°E)
F1	22	15.6	48.0	9.4	27.48	76.3	112.2
F2	23	16.7	40.4	9.2	29.94	74.1	134.6
F3	20	19.8	48.7	8.1	35.21	72.6	110.0
Summation	65	–	–	–	–	–	–
Mean	–	17.3	45.7	7.4	280.72	74.7	119.4

***Key*; N**: Number of specimens exhibit the specific component, **D**: Declination, I: Inclination, **α_{95}**: Radius of 95% circle of confidence (Fisher 1953) for mean direction, **K**: Precision parameter (Fisher 1953), **P_Lat, P_long**: Latitude and longitude of the Virtual Geomagnetic Pole. Mean calculated using Remasoft 3.0 computer program (2018).

Table 2. Demagnetization results of the Hard Ores.

Site No.	N	D (°)	I (°)	α_{95} (°)	K	P_Lat. (°N)	P_Long. (°E)
R1	14	184.8	−39.8	10.2	82.63	82.9	170.6
R2	10	191.9	−29.5	1.8	59.85	73.4	165.4
R3	10	185.8	−39.9	9.6	64.35	82.4	164.7
R4	11	193.6	−30.2	11.3	46.68	72.7	160.3
Summation	45	–	–	–	–	–	–
Mean(Hn)	–	189.3	−34.9	7.7	142.58	77.6	164.0
R5	8	26.9	41.6	10.1	149.70	65.5	123.3
R6	8	22.0	40.1	11.1	94.30	69.7	129.7
Summation	16	–	–	–	–	–	–
Mean(Hr)	–	24.4	40.9	8.7	320	67.6	126.2
Summation	61	–	–	–	–	–	–
Mean (total)	–	14.1	37.1	7.3	20.7	75.2	146.7

Notations as in Table 1

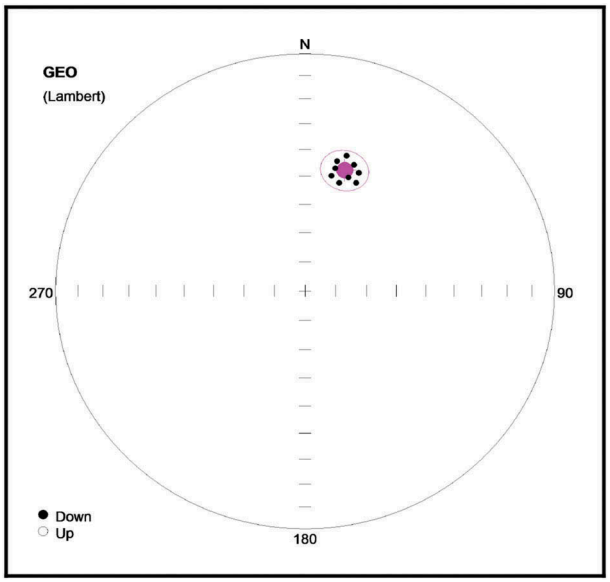

Figure 11. Stereographic projection of the overall mean direction of the Friable Ores.

The magnetic components isolated from the Friable Ore show a normal polarity (Figure 11). The overall mean direction is, Dec. = 17.3°, Inc. = 45.7°, α_{95} = 7.4°. The corresponding VGP lies at Lat. = 74.7° N and Long. = 119.4° E (Table 1). The obtained components were clustered on the stereonet of (Figure 11).

The mean direction obtained for the two groups, after inverting the reversed polarity to normal polarity, is, Dec. = 14.1°, Inc. = 37.1°, and α_{95} = 7.3°, with corresponding paleopole lies at Lat. = 75.2° N and Long. = 146.7°E (Table 2). The obtained component overall the mean direction is shown on the stereonet of (Figure 12).

6. Magnetic fabric

The measurement of anisotropy of the low-field magnetic susceptibility (AMS) was performed, using the KAPPABRIDGE (MFK1-FA). The method principally involves the collection of orientated rock specimen, followed by the measurement of strength of the induced magnetization that a sample acquires when a magnetic field is applied at different orientations. Any difference can be interpreted in terms of the net shape of the grains, and the degree of their crystalline alignments, which in turn, can be interpreted in the same way as in all other petrofabric techniques). All the measurements have been done with a pattern of the Jelinek's design of the 15 directions of measurements (Tauxe 1998). The results of the measurement, in the form of various parameters derived from the susceptibility tensor and orientations of the directions of the principal susceptibilities in various coordinate systems, are presented on the screen. The results of these measurements were analysed using *Anisoft* software package (Lotfy et al. 2017).

Tables 3 and 4 are the summary results of the measurements of AMS, for the Friable and Hard Ores.

Measurements of the magnetic susceptibility at room temperature and its anisotropy (AMS) showed that, the average susceptibility equals 572×10^{-6} SI unit (Table 3). The low anisotropy degree *(P')*, indicates a very low deformation, and have dominated sedimentary depositional component. The magnetic foliation is predominance over lineation. The obtained low (*P'*) oblate shape AMS ellipsoid and the distribution of maximum (K_1) and minimum (K_3) susceptibility axes on equal area projection confirm the primary sedimentary fabric. Although the anisotropy is low, the magnetic foliations

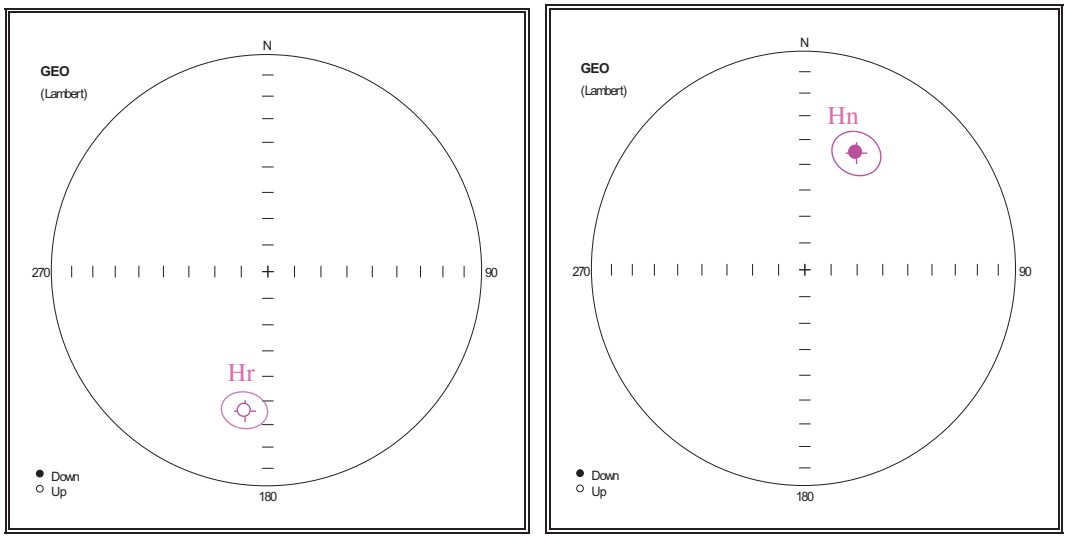

Figure 12. Stereographic projection of the overall mean direction of the Hard Ores (Hn-normal polarity on the right and Hr-reverse polarity on the left).

Table 3. Site-mean magnetic susceptibility and AMS data for the Friable Ores.

Site	N	K_m ($*10^{-6}$ SI unit)	P'	T	L	F	Magnetic susceptibility axes for mean tensor K_1	K_2	K_3
F1	15	518	1.005	0.302	1.002	1.004	189/1	99/3	292/87
F2	11	543	1.004	0.273	1.001	1.003	345/7	255/6	124/81
F3	7	735	1.003	−0.194	1.002	1.002	127/10	223/29	21/59
Summat-ion	33	–	–	–	–	–	–	–	–
Mean		572	1.004	0.187	1.001	1.003	–	–	–

Key: N: number of specimens. K_m: mean susceptibility = $(K_1 + K_2 + K_3)/3$, in 10^{-6} SI. ***P'***: anisotropy degree = $exp\sqrt{\{2[(\eta_1-\eta_m)^2 + (\eta_2-\eta_m)^2 + (\eta_3-\eta_m)^2}$ Where: $\eta_1 = ln\ K_1$, $\eta_2 = ln\ K_2$, $\eta_3 = ln\ K_3$ and $\eta_m = \sqrt[3]{\eta_1.\eta_2.\eta_3}$
T: ellipsoid shape = $[2\ ln\ (K_2/K_3)/ln\ (K_1/K_3)] - 1$ ***L***: magnetic lineation = K_1/K_2. ***F***: magnetic foliation = K_2/K_3.

Table 4. Site-mean magnetic susceptibility and AMS data for the Hard Ores.

Site	N	K_m ($*10^{-6}$ SI unit)	P'	T	L	F	Magnetic susceptibility axes for mean tensor K_1	K_2	K_3
R1	9	1050	1.005	0.197	1.002	1.003	312/5	43/3	160/84
R2	6	1200	1.006	0.051	1.002	1.004	86/13	354/6	240/76
R3	12	228	1.019	0.222	1.007	1.012	292/10	201/3	97/79
R4	3	755	1.007	0.433	1.002	1.005	39/13	130/3	232/77
R5	15	804	1.003	0.815	1.000	1.003	16/1	286/23	106/67
Summ-atio	45	–	–	–	–	–	–	–	–
Mean	–	813	1.006	0.402	1.002	1.005	– -	– -	– -

Notations as in Table 3

with slightly girdle-distributed (K_3) axes are consistent between sites (*F1*) and (*F2*). Together with (K_1) magnetic lineation, may suggest some secondary tectonic (deformational component) to the AMS. Also, for (*F3*) site, the mean axes of AMS can be influenced by the same tectonic component, although it is probably affected by changes in composition (Figure 13).

The magnetic susceptibility of the hard ores is rather variable (Figure 14), this indicates some variation in the content of magnetic minerals. The average susceptibility equals 813×10^{-6} SI unit (Table 4). The tensor of mean AMS data was calculated for five sites and approximated for site R4 (as the little numbers of specimens). The low anisotropy degree *(P')*, indicates a very low deformation, and have dominated sedimentary depositional component. The magnetic foliation is predominance over lineation and the susceptibility ellipsoid is clearly oblate, with positive value of the shape parameter, (*T*).

Although the anisotropy is low, the magnetic foliations with slight girdle are consistent between the sites R1, R2 and R3. Together with NW-SE trending (K_1) magnetic lineation, may suggest some weak secondary tectonic (deformational NE-SW component) to AMS. Also for R5 site, the mean axes of AMS can be influenced by the same weak tectonic component, although the sense of deformation can slightly different that for R1-R3 (NW-SE compression).

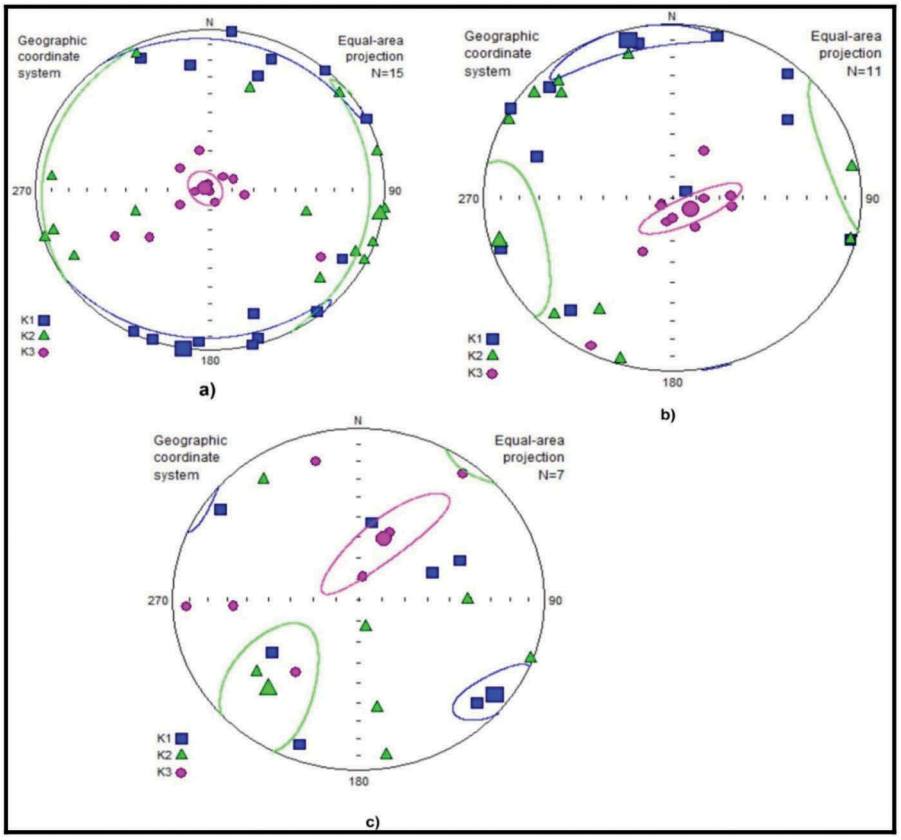

Figure 13. Equal-area projection of the in-situ directions of magnetic susceptibility principal axes for sites from Friable Ores.

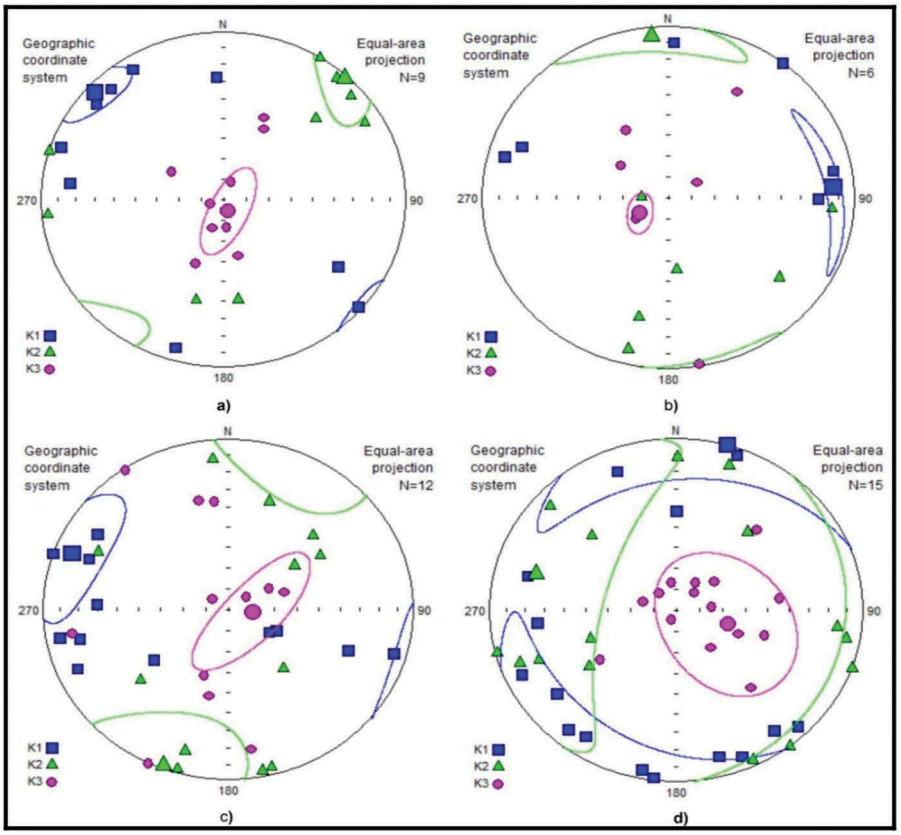

Figure 14. Equal-area projection of the in-situ directions of magnetic susceptibility principal axes for sites from Hard Ores.

7. Discussion

In this paper, we relied mostly on the Thermal Demagnetization; according to the demagnetization results, the studied ores carry a stable single magnetic component, of Middle Eocene age. The results obtained from the rock magnetic studies and thermal demagnetization reveal the coexistence of haematite as the main magnetic carrier of NRM. Tables 1 and 2 summarize the mean values of the obtained components.

The magnetic components obtained from the demagnetization processes of the Friable Ore are composed of a single magnetic component. This single component is stable, carried by haematite and shows a normal polarity. Demagnetization of the studied specimen from the Hard Ore shows a single and stable component with normal and reverse polarities. The presence of normal and reverse polarities carried by hematite can be understood in the light of the geomagnetic polarity timescale of Gradstein et al. (2012) Figure (15), where the geomagnetic field had normal and reversed polarities at that period.

The overall mean direction, that obtained from the Friable Ores and Hard Ores, is, Dec. = 15.1°, Inc. = 40.0°, and α_{95} = 5.5°, with paleopole lies at Lat. = 75.3° N, Long. = 137.9° E (Table 5).

When we compared the resultant palaeomagnetic pole from the Friable and Hard Ores with the other poles of the Eocene age in Egypt (Table 6) and

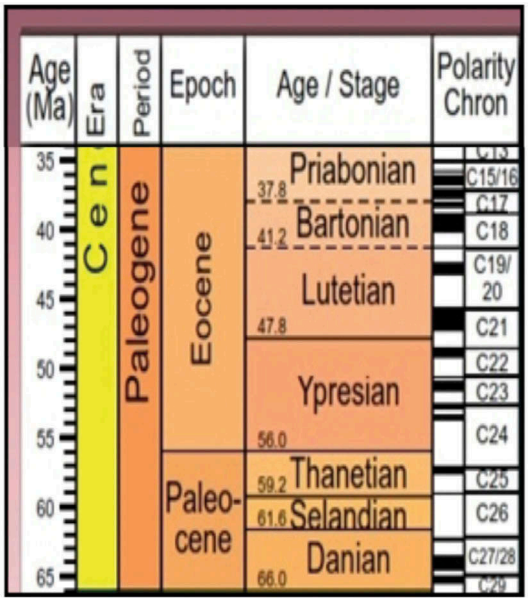

Figure 15. The geologic timescale of Gradstein et al. (2012).

Table 5. Mean directions and pole positions for the Friable and Hard Ores.

Ores Type	N	Dec°	Inc.°	α_{95}	Pal_Lat	P_Lat. °N	P_Long. °E
Friable Ores	3	17.3	45.7	7.4	27.1	74.7	119.4
Hard Ores	6	14.1	37.1	7.3	20.7	75.2	146.7
Mean	9	15.1	40.0	5.5	22.8	75.3	137.9

Notations as in Table 1

Table 6. Some selected Eocene pole positions of Egypt.

Pole	Rock unit, Location	Paleopole Lat. (°N)	Paleopole Long. (°E)	α_{95}	Reference
1	Mokattam limestone	73	147	11.2	Kafafy et al.
2	Maadi limestone	75	150	14.7	(1995)
3	Mokattam	78	163	4.1	Kafafy et al.
4	limestone (Friable and Hard Ores), Bahariya oasis	75	138	5.5	(1995) Abdeldayem (1999) This study

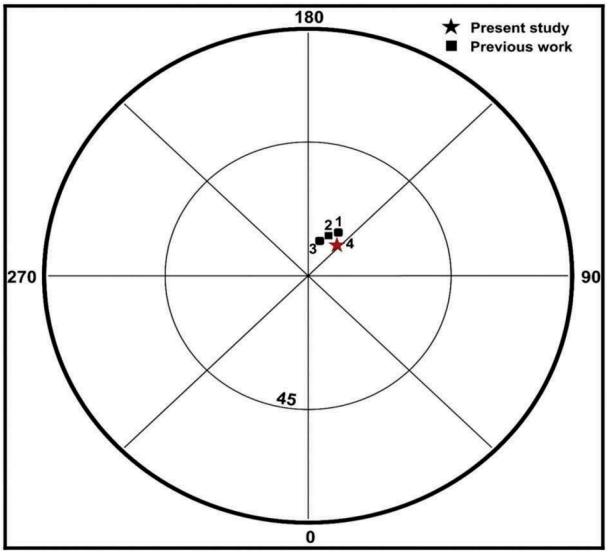

Figure 16. Some selected Eocene poles with the pole of the present study.

(Figure 16), we found that there is a good agreement between them and the resultant pole is of primary origin (Perrin and Saleh 2018).

The magnetic fabric results show that the magnetic anisotropy is low and have a dominate primary sedimentary depositional component. However, a slight secondary weak tectonic component can be also recognized, that may be caused by NE-SW compression with the development of weak NW-SE sub horizontal lineation. The direction of the principle magnetic susceptibility axes is fairly scattered with variable degree of inclination, reflecting a weak magnetic fabric. Weak AMS fabric is rather indicative that the ore was originated in the process of sedimentation and later compaction.

8. Conclusion

Palaeomagnetic and magnetic fabric studies of the Bahariya iron ores deposits have been proven to be a powerful tool for inferring the age and origin of these deposits. The following conclusions may be drawn concerning the age and origin of the Bahariya iron ores deposits:

(1) The age of the different ores types is the same, as their host rocks. The Naqb-Qazzun (Friable and Hard Ores), have a primary magnetic component

of Middle Eocene age, where the host rock is Naqb-Qazzun Formation (Lutetian).

(2) Measurements of the magnetic susceptibility and its anisotropy resulted from the studied ores types have been originated during sedimentation. Both ore types are of sedimentary deposition (supergene origin), including the direct of precipitation from seawater and/or leaching of the underlying Nubia sandstones and basement rocks.

Disclosure statement

No potential conflict of interest was reported by the authors.

ORCID

A. Khashaba http://orcid.org/0000-0001-6359-0464
R. Mostafa http://orcid.org/0000-0002-8850-4056

References

Abdeldayem AL. 1999. Palaeomagnetism of some Cenozoic sediments, Cairo-Fayum area, Egypt: phys. Earth Planet Inter. 110:71–82.

Abdel-Monem AA, Korany EA, Yousef AM. 2003. Occurrence and genesis of pyrite in El Gedida Mine, El Bahariya depression, Western Desert, Egypt. Sedimentology Egypt. 11:227–238.

Baioumy HM, Ahmed AH, Khedr MZ. 2014. A mixed hydrogenous and hydrothermal origin of the Bahariya iron ores, Egypt: evidences from the trace and rare earth element geochemistry. J Geochemical Exp. 146:149–162.

Baioumy HM, Hassan MS. 2004. Authigenic halloysite from El Gedida iron ores, Bahariya oasis, Egypt: characterization and origin. Clay Miner. 39:207–217.

Catuneanu O, Khalifa MA, Wanas HA. 2006. Sequence stratigraphy of the lower cenomanian Bahariya formation, Bahariya oasis, Western Desert, Egypt. Sediment Geol. 190:121–137.

Dabous AA. 2002. Uranium isotopic evidence for the origin of the Bahariya iron deposits, Egypt. Ores Geol Rev. 19:165–186.

El Sharkawi MA, Higazi MM, Khalil NA (1984): Three genetic iron ores dikes of iron ores at El Gedida mine, Western Desert. Egypt. Geol. Soc. Egypt. 21st Annual Meeting, Cairo, Egypt (Abstract).

El-Aref MM, El Sharkawi MA, Khalil MA 1999. The geology and genesis of stratabound to stratiform Cretaceous-Eocene iron ore deposits of El Bahariya Region, Western Desert, Egypt. International Conference on Geol. Arab World (GAW4); p. 450–475.

El-Aref MM, Lotfy ZH. 1985. Genetic karst significance of the iron ore deposits of El Bahariya Oasis, Western Desert, Egypt. Ann Geol Surv Egypt. 15:1–30.

El-Shazly EM. 1962. Report on the results of drilling in the iron ore deposit of Gebel Ghorabi, Bahariya Oasis, Western Desert. Geol Surv Egypt. 17: 25.

Fisher RA. 1953. Dispersion on a sphere. Proc: R Soc London Ser. 217:295–305.

Gradstein FM, Ogg JG, Schmitz M, Ogg GM. 2012. The geologic time scale. The website of the Geologic Time Scale Foundation (published by Elsevier).

Helba H, Khalil K, Abou N. 2001. Alteration patterns related to hydrothermal gold mineralizaition in meta-andesites at Dungash area, Eastern Desert, Egypt. Resour Geol. 51(1):19–30. doi:10.1111/rge.2001.51.issue-1

Hermina M, Klitsch E, Lift F. 1989. Stratigraphic lexicon and explanatory notes to the geological map of Egypt, 1: 500000. Cairo (Egypt): Conoco Inc; p. 263.

Hussein A. 1990. Mineral deposits. In: Said R, editor. The Geology of Egypt. London: Taylor and Francis Publishers; p. 511–566.

Kafafy AM, Tarling DH, El-Gamili MM, Hamama HH, Ibrahim EH. 1995. Contributions to the Cretaceous-Tertiary palaeomagnetism in the Nile Valley, Egypt: proc. Egypt Acad Sci. 45:121–139.

Lotfy H, Abu Heleika M, Mostafa R, Wahbah D. 2017. Africa was still far south in the Late Ypresian: paleomagnetic study on the Early Eocene 'Minia' Formation in central Egypt. NRIAG J Astron Geophys. 6:336–348.

Morsy MA (1989): Geology and radioactivity of Late Cretaceous-Tertiary sediments in the North Western Desert, Egypt [PhD. Thesis, Fac. of Science]. Mansoura Univ; p. 175.

Perrin M, Saleh A. 2018. Cenozoic to Cretaceous paleomagnetic dataset from Egypt: new data, review and global analysis. Earth Planet Sci Lett. 488:92–101.

Plyusnina EE, Sallam ES, Ruban DA. 2016. Geological heritage of the Bahariya and Farafra oases, the central Western Desert of Egypt. J Afr Earth Sci. 116:151–159.

Remasoft 3.0 computer program. 2018. http://www.agico.com.

Said R. 1990. The geology of Egypt. Rotterdam/rookfield: A. A. Balkema; p. 159.

Schult A, Soffel H, Hussain AG. 1978. Paleomagnetism of Cretaceous Nubian Sandstone. J Geophy. 44:333–340.

Tauxe L. 1998. Paleomagnetic principles and practice. Dordrecht: Kluwer Academic Publishers.

Tosson S, Saad NA. 1974. Genetic studies of El-Bahariya iron ores deposits, Western Desert, Egypt. Neus Jahrb Fur Mineral-Abh. 121:317–393.

Zijderveld J. 1967. A.C. demagnetization of rocks-analysis of results. In: Colllinson DW, Creer KM, Runcorn SK, editors. Methods in rock magnetism and paleomagnetism. Amsterdam (The Netherlands): Elsevier; p. 254–286.